

COMMUNICATION

Assembly Architecture and DNA Binding of the Bacteriophage P22 Terminase Small Subunit

Daniel Němeček¹, Gabriel C. Lander², John E. Johnson²,
Sherwood R. Casjens³ and George J. Thomas Jr^{1*}

¹*School of Biological Sciences, University of Missouri-Kansas City, 5100 Rockhill Road, Kansas City, MO 64110-2499, USA*

²*Department of Molecular Biology, The Scripps Research Institute, 10550 North Torrey Pines Road, La Jolla, CA 92037, USA*

³*Division of Cell Biology and Immunology, Department of Pathology, University of Utah Medical School, Salt Lake City, UT 84112, USA*

Received 18 June 2008;
received in revised form
11 August 2008;
accepted 20 August 2008
Available online
27 August 2008

Morphogenesis of bacteriophage P22 involves the packaging of double-stranded DNA into a preassembled procapsid. DNA is translocated by a powerful virally encoded molecular motor called terminase, which comprises large (gp2, 499 residues) and small (gp3, 162 residues) subunits. While gp2 contains the phosphohydrolase and endonuclease activities of terminase, the function of gp3 may be to regulate specific and nonspecific modes of DNA recognition as well as the enzymatic activities of gp2. Electron microscopy shows that wild-type gp3 self-assembles into a stable and monodisperse nonameric ring. A three-dimensional reconstruction at 18 Å resolution provides the first glimpse of P22 terminase architecture and implies two distinct modes of interaction with DNA—involving a central channel of 20 Å diameter and radial spikes separated by 34 Å. Electromobility shift assays indicate that the gp3 ring binds double-stranded DNA nonspecifically *in vitro* via electrostatic interactions between the positively charged C-terminus of gp3 (residues 143–152) and phosphates of the DNA backbone. Raman spectra show that nonameric rings formed by subunits truncated at residue 142 retain the subunit fold despite the loss of DNA-binding activity. Difference density maps between gp3 rings containing full-length and C-terminally truncated subunits are consistent with localization of residues 143–152 along the central channel of the nonameric ring. The results suggest a plausible molecular mechanism for gp3 function in DNA recognition and translocation.

© 2008 Elsevier Ltd. All rights reserved.

Edited by M. Gottesman

Keywords: P22 bacteriophage; terminase structure; DNA binding; electron microscopy; Raman spectroscopy

In the assembly of a double-stranded DNA (dsDNA) bacteriophage the viral genome is packaged into a capsid precursor (procapsid) through the action of an enzyme complex called terminase. The complex is so named because its nucleolytic activity cleaves over length replicating DNA to establish the termini of the packaged viral genome. Similar packaging mechanisms occur in *Herpesviridae* and other eukaryotic dsDNA viruses. Typically, the terminase contains two types of subunits, which are responsible for DNA recognition, phosphohydrolysis, and translocation.¹ For the well-studied bacteriophages P22, SPP1, T3, T4, T7, and λ, the larger of the two terminase subunits

exhibits the required phosphohydrolase and translocase activities,^{2–9} while the smaller subunit is involved in the identification of the dsDNA packaging initiation sites (usually called *pac* or *cos*)^{10–12} and presumably in enzymatic regulation of the large subunit.^{3–6,10} Small terminase subunits are more variable in amino acid sequence than the large subunits (S. R. Casjens, unpublished results) and it is not known if all are true homologues or have structures with different origins. In the case of P22, the terminase small subunit (gp3, 162 amino acids, 18.6 kDa) and large subunit (gp2, 499 amino acids, 57.6 kDa)^{13,14} function in concert to package DNA by a “headful” mechanism that is initiated through recognition of a specific DNA packaging signal (*pac* site).^{15–17} Similar mechanisms have been proposed for the terminases of phages SPP1 and T4.^{18,19} A common theme in all of these dsDNA phages is the participation of the

*Corresponding author. E-mail address:
thomasgj@umkc.edu.

Abbreviations used: dsDNA, double-stranded DNA; EM, electron microscopy.

terminase large and small subunits in a ternary complex with the appropriate packaging initiation site. To form the functional terminase/*pac* complex, the terminase small subunit of SPP1 (G1P) assembles into an approximately decameric ring,⁵ while those of T4 (gp16) and T7 (gp18) are reported to assemble into approximately octameric rings.^{20–22} The terminase small subunit of phage λ , on the other hand, has been proposed to form a dimer alone in solution and bind to specific sequences within the *cos* site of the λ genome in the form of a hetero-oligomeric ring constructed from a 2:1 ratio of small (gpNu1) and large (gpA) subunits.^{23,24} While cleavage of λ *cos* is required for packaging, the precise roles of the proposed terminase ring and its heterotrimeric precursor are not known.

A three-dimensional atomic structure has been determined by nuclear magnetic resonance for the N-terminal DNA binding domain of the phage λ small terminase subunit.²⁵ However, the protein fold has not yet been determined for the full-length small subunit of any terminase. While oligomeric ring formation may be common among the small terminase subunits of many dsDNA phages, no detailed ring structure or uniform oligomer size has yet emerged. Recently, we reported the conformational properties, assembly states, and DNA-binding activities of the small (gp3) and large (gp2) subunits of P22 terminase. Two-dimensional averaging of negatively stained gp3 particles revealed a nonameric ring structure for the wild-type protein and a decameric ring structure for the mutant Ala 112→Thr.²⁶ Here, we further characterize DNA binding properties of wild-type gp3 and report the first three-dimensional reconstructions of a terminase small-subunit assembly by resolving to 18 Å the nonameric ring structure of wild-type gp3. The structure provides new insights into the architecture of the P22 DNA translocation machine and suggests a molecular mechanism for DNA packaging.

Preparation and purification of gp3 constructs

The plasmid construct employed for overexpression of full-length wild-type gp3 in *Escherichia coli*, the methods used for isolation and purification of the recombinant protein, and the demonstration of DNA packaging activity in *Salmonella* infections have been described.²⁶ The full-length construct contained a 20-amino-acid N-terminal addition consisting of a histidine tag (His₆) and thrombin cleavage site encoded by the pET-15b expression vector plasmid. The N-terminal addition was removed prior to final purification of the protein.²⁶ The plasmids used for overexpression of truncated variants of gp3 were made as site-directed deletions of the plasmid used for expression of full-length gp3 (QuikChange® Site-Directed Mutagenesis Kit strategy with PFU ULTRA® DNA polymerase, Stratagene, La Jolla, CA). Expression and purification of gp3 truncates followed the same protocols used for the full-length protein.

Locus of the nonspecific DNA binding activity of gp3

DNA binding properties of the gp3 nonamer in the presence of a 50-bp DNA target that incorporated either the native 21-bp *pac* site or a functionally inactive permuted *pac* site were assayed previously by native gel electrophoresis.²⁶ Similar gp3 binding affinities were observed for both DNA targets, indicating the formation of *nonspecific* gp3/DNA complexes. This is consistent with the expectation that genome translocation requires of terminase a nonspecific mode of DNA recognition in addition to *pac* site recognition. Also consistent with this interpretation is the observation that both of the 50-bp DNA targets are capable of binding several nonameric gp3 rings when excess nonamer is present (data not shown).

To address the question of whether the highly basic C-terminal region of the 162-residue gp3 subunit¹⁴ might be the locus of nonspecific DNA recognition, we constructed plasmids for overexpression of C-terminal truncations of gp3. Two C-terminal truncates, lacking 10 and 20 amino acids

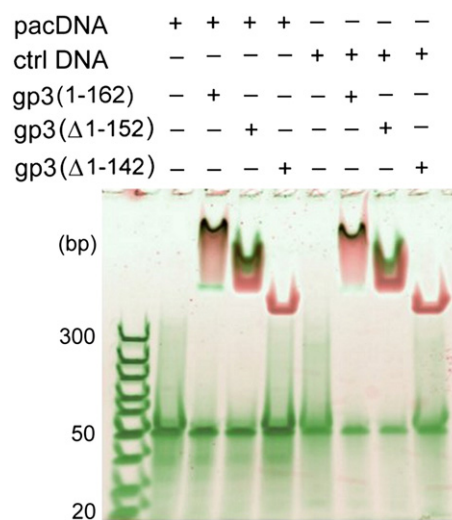


Fig. 1. The binding of full-length and C-terminally truncated gp3 rings to 50-bp DNA targets incorporating either the 21-bp *pac* site or a permuted (nonfunctional) sequence of the same AT/GC content²⁶ was examined by native gel electrophoretic mobility shift assay. Mixtures of DNA and gp3 rings were incubated at room temperature for 30 min and loaded onto a 4–20% polyacrylamide gel. The total DNA concentration in each lane was 200 nM. DNA and protein were stained with SYBR Green and SYPRO Ruby fluorescent dyes, respectively, and the gel was scanned with a Typhoon 9400 Scanner (Amersham Biosciences, Piscataway, NJ). The DNA-free gp3 ring appears at the top of the gel, and protein-free DNA (50 bp) migrates to the middle of the gel. DNA/gp3 complexes are visualized as dark spots. The full-length and truncated gp3 rings progress differently into the gel due to the different net charges of the respective rings. While rings assembled from full-length gp3 and the gp3 (Δ 1–152) truncate bind DNA comparably, no DNA binding is observed for the gp3(Δ 1–142) ring.

and designated, respectively, as gp3(Δ 1–152) and gp3(Δ 1–142), exhibited stable subunit folds (Raman data shown below), the same nonameric oligomer state as the full-length protein (mass spectrometric data not shown), yet distinctly different nonspecific DNA-binding activities. The former contains a net charge of -1 relative to full-length gp3, while the latter contains a net charge of -5 relative to full-length gp3. The similarity in charges of gp3(Δ 1–152) and full-length gp3 leads to comparable DNA binding, while the removal of 20 C-terminal amino acids in gp3(Δ 1–142) results in the complete loss of DNA binding (Fig. 1). Evidently, the highly basic sequence 143 RDKRRSRIK that is removed by the deletion of amino acids 143–151 plays an important electrostatic role in nonspecific DNA recognition and binding.

The fold of C-terminally truncated gp3

Raman spectra of nonameric assemblies of full-length and C-terminally truncated gp3 (lacking either 20 [gp3(Δ 1–142)] or 10 [gp3(Δ 1–152)] residues) exhibit very similar amide I (1658 cm^{-1}) and amide III (1253 cm^{-1}) markers, as shown in Fig. 2a. This suggests that the subunit fold is largely conserved after removal of residues 143–162. Quan-

titative analysis²⁷ of the amide I band profile of the gp3(Δ 1–142) truncate indicates $39\pm 2\%$ α -helix, $21\pm 2\%$ β -strand, and $40\pm 3\%$ irregular structure, which differs only marginally from the secondary-structure distribution in full-length gp3.²⁶ The weak positive difference peaks, which are centered within the amide I band envelope near 1648 and 1677 cm^{-1} , are consistent with the presence of ordered α -helical and β -strand secondary structures, respectively, in the C-terminal 20 residues of gp3.

The tyrosines (Tyr35, Tyr52, Tyr86, Tyr104) and tryptophans (Trp10, Trp29, Trp38, Trp45, Trp83) of gp3 are located in the region of the sequence that is present in all three variants, and their Raman markers are potentially informative of any tertiary structural changes that might result from the C-terminal truncations. Figure 2a shows that the diagnostic Raman doublets of the tyrosines ($828/853\text{ cm}^{-1}$)^{28,29} and tryptophans ($1340/1360\text{ cm}^{-1}$)³⁰ of gp3(Δ 1–142) are similar to those of full-length gp3. This supports the conclusion that the tertiary structure within residues 1–142 is largely invariant to the C-terminal truncations. The small spectral differences between gp3(Δ 1–142) and full-length gp3, which are revealed as positive difference bands in the three times amplified difference spectrum of Fig. 2a, can be assigned confidently to the excised side chains of the 143–162 sequence.³¹ Notable

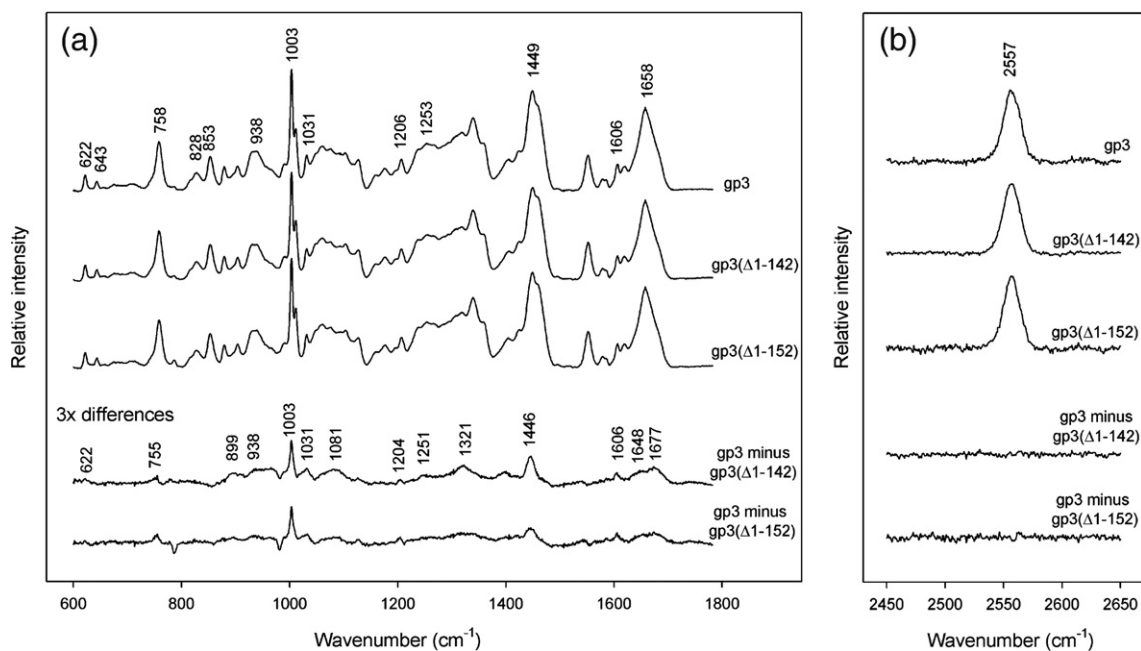


Fig. 2. Raman spectroscopy of nonameric ring assemblies of the full-length wild-type gp3 protein and C-terminal truncates gp3(Δ 1–142) and gp3(Δ 1–152). Solutions of purified rings were concentrated to $\sim 20\text{ mg/mL}$ in 10 mM Tris (pH 7.8), 0.1 M NaCl and sealed in 1-mm glass capillaries maintained at 20°C . Raman spectra were excited at 532 nm (Verdi-5 laser, Coherent, Palo Alto, CA) and collected in the 90° scattering geometry (Spex 500M spectrograph, JY Horiba, Edison, NJ). Standard corrections for contributions of the buffer and glass were applied.²⁶ (a) From top to bottom: spectra in the region $600\text{--}1800\text{ cm}^{-1}$ of rings formed by full-length gp3, C-terminal truncate gp3(Δ 1–142), C-terminal truncate gp3(Δ 1–152), corresponding difference spectra (amplified threefold) between full-length and truncated species, as labeled. The integrated intensity of the tyrosine marker at 643 cm^{-1} was employed as the internal intensity standard. (b) From top to bottom: spectra in the region $2450\text{--}2650\text{ cm}^{-1}$ of rings formed by full-length gp3, C-terminal truncate gp3(Δ 1–142), C-terminal truncate gp3(Δ 1–152), and corresponding difference spectra, as labeled. The integrated intensity of the 2557 cm^{-1} band was employed as the internal intensity standard.

among these are the difference peaks at 622, 755, 1003, 1031, 1081, 1204, and 1606 cm^{-1} , all of which are attributed to the excised Phe154 residue, and the difference peaks near 885, 936, and 1321 cm^{-1} , which are due primarily to arginines and lysines of the excised C-terminus.

Each cysteine (Cys32, Cys33) of gp3 is also expected to generate a Raman marker that is informative of the local environment of the side-chain sulfhydryl (S–H) group.³² The single symmetrical band observed at 2557 cm^{-1} (Fig. 2b) in the full-length gp3 assembly indicates that the S–H donors of Cys32 and Cys33 are not exposed to the aqueous solvent but participate in robust S–H \cdots X interactions with other protein acceptor groups. These interactions are unaffected by C-terminal truncations. Strong S–H \cdots X bonding by the Cys32 and Cys33 side chains suggests that this region of the gp3 chain is either buried within the subunit fold or protected from solvent exposure by the intersubunit interface. The results are also consistent with very little change in the subunit fold after removal of residues 143–162, as noted above.

The spectral differences observed between the gp3 (Δ 1–152) truncate and full-length gp3 (Fig. 2) are consistent with the above results. In combination with the gel binding assays of Fig. 1, the Raman spectra thus show that (i) the region of the gp3 sequence responsible for nonspecific DNA recogni-

tion (residues 143–162) adopts a stable α/β fold, and (ii) excision of the putative DNA binding segment does not appreciably perturb either the secondary or tertiary structure of the remaining gp3 sequence (i.e., residues 1–142).

Three-dimensional structure of the gp3 assembly

Recently, we reported that the terminase small subunit of P22 assembles into a highly stable and symmetric ring.²⁶ Two-dimensional averaging of the gp3 assemblies identified in electron micrographs of negatively stained particles revealed a central hole of approximately 20 Å in diameter with electron density emerging radially from the central annulus. Here, we have further analyzed the structure of the gp3 ring assembly by three-dimensional single-particle analysis of negatively stained gp3 ring particles.

The three-dimensional reconstruction of the gp3 assembly at 18 Å resolution, as reported by RMEASURE,³³ reveals a morphology that is roughly funnel-like in shape, being much wider at one end than the other (Fig. 3a). Despite the relatively low

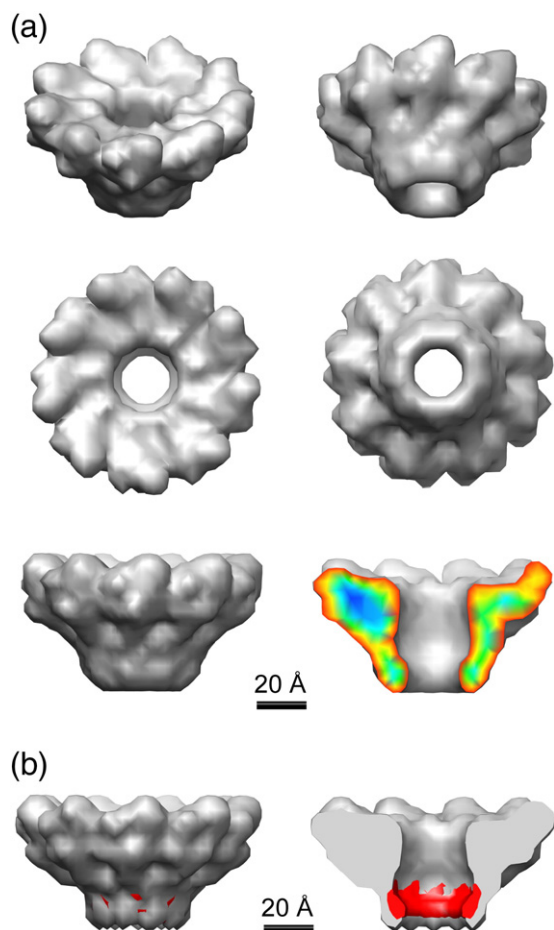


Fig. 3. (a) 3D reconstruction of the gp3 ring assembly from negatively stained particles. The map was rotated 30° about the horizontal axis in the top two images, and viewed from above and below in the central images. The funnel-like morphology is evident when viewed from the side in the lowest two images, and a cutaway view on the right is colored by density strength. The ringlike structure of gp3 is clearly divided into two domains—the wider spike domain, in which 9 protrusions can be seen reaching out from the central channel at a skewed orientation, and the annulus domain, which forms a thin-walled channel extending away from the spike domain. The central channel accommodates the passage of double-stranded (*B* form) DNA, as shown in Fig. 4a, with a slightly smaller opening at the annulus than at the spike domain. Dimensions are listed in Table 1. The 9-fold symmetry of the wild-type gp3 particles discerned in previous negative stain work was confirmed by performing a reference-free classification of selected top view particles. The resulting class averages presented only 9-fold views, without the enforcement of symmetry. To rule out the possibility of symmetrization bias, we performed separate 3D reconstructions enforcing either 8-fold (C8), 9-fold (C9), or 10-fold (C10) symmetries, each with a single radially averaged starting model. While the C8 and C10 reconstructions resulted in smooth featureless ringlike densities, the C9 reconstruction showed structural details for which the top-view projections matched those of the reference-free classification. Further discussion of the assembly architecture and its relevance to terminase function are discussed in the text. (b) 3D reconstruction (side and cutaway views) of the nonameric truncated gp3(Δ 1–127) ring, along with the difference density shown in red. This difference, which corresponds primarily to the C-terminal 35 amino acids (see text), suggests that the C-terminal residues involved in nonspecific DNA recognition are localized mainly along the inner surface of the central channel.

resolution of this structure, certain features and dimensions can be clearly distinguished. Protruding structures approximately 27 Å in height surround the wider end or mouth of the funnel, extending a distance of 38 Å from the inner edge at the narrowest opening of the central channel. Although these “spikes” have a definite skewed appearance relative to the central channel, the handedness of the reconstruction cannot be determined without further experiments. The spike domain of the structure accounts for nearly 80% of the total mass of the ring assembly and, due to its complexity, is likely to be involved in multiple recognition events (see below). The annulus region, which may be important for intersubunit association and DNA passage, may also provide surfaces for binding of gp2 or other proteins involved in the formation of an active translocation complex. Given that the electron density of proteins correspond on average to 0.8 Da/Å³, the reconstructed density was depicted at a contour level corresponding to 167.4 kDa (the mass of nonameric gp3). At this contour level salient features of the structure emerge, including an overall height of 57 Å and a maximum outer diameter of 99 Å in the spike domain that narrows to a diameter of 49 Å at the annulus. At the funnel mouth (top surface as oriented in the bottom images of Fig. 3a), the central channel entrance has a diameter of ~25 Å. This opening widens slightly to ~28 Å before narrowing to ~20 Å in diameter at the neck of the annulus domain. The channel appears to be sufficient to accommodate the passage of B-form DNA. The height of the channel opening between the neck and mouth of the funnel is roughly 42 Å. (See also Table 1).

The elongated subunit shape in the gp3 assembly (Fig. 3a, bottom right) implies a multidomain structure in which at least one domain (the central annulus) plays a role in subunit/subunit recognition and one or more domains interact with DNA, with the terminase large subunit (gp2), and possibly with the DNA entry channel of the procapsid (portal protein, gp1). Details of these structure–function relationships remain to be determined. Our reconstruction shows, however, that the subunit electron density is significantly elongated in a direction close to perpendicular to the plane of the ring, thus providing a channel with large surface area for recognition and/or passage of agents of appropriate cross-sectional diameter (~20 Å).

Table 1. Dimensions of the reconstructed gp3 ring

Outer diameter (Å)	
Spike domain	99
Annulus	49
Inner diameter (Å)	
Spike domain	25
Annulus	20
Maximum channel diameter (Å)	28
Channel height (Å)	42
Overall height (Å)	57

Location of the gp3/DNA interface

Figures 1–3 show that the excision of gp3 residues 143–162 eliminates nonspecific DNA binding, but does not impact either the native subunit fold of residues 1–142 or the overall nonameric ring structure that is visualized by negative-stain electron microscopy (EM). We attempted to further localize the nonspecific DNA-binding interface of gp3, within the context of the ring assembly, by computing a protein density difference map between rings consisting of full-length gp3 and the truncated gp3(Δ1–142). However, the result was inconclusive (data not shown), owing to the relatively small mass difference between rings consisting of the full-length and truncated subunits (<22 kDa). We therefore examined the difference between reconstructed rings of full-length gp3 and the more radically truncated variant gp3(Δ1–127). The greater mass differential in this case (~37 kDa) does allow visualization a part of the truncated C-terminus in the computed difference map, as shown in Fig. 3b. The external and cutaway side views of Fig. 3b indicate that at least a portion of the 35 amino acids of the gp3 C-terminus (¹²⁸KEQSQVEDVTPDKGDRDKRRSRIKELFNRTGRDS), which includes the interface for nonspecific DNA recognition, is localized principally along the inner surface of the central channel and proximal to the neck opening.

Function of gp3 in the DNA packaging machine

The overall dimensions of the reconstruction of Fig. 3a are given in Table 1. These parameters suggest intriguing possibilities for DNA binding, *pac* site recognition, and genome translocation. For example, the central hole of the gp3 ring exhibits a diameter that is appropriate to the passage of dsDNA. It could thus provide a DNA-translocating channel that is dimensionally compatible with the translocating channel of the procapsid portal. The likely location of gp3 sites of nonspecific DNA binding activity (residues 142–162) along this channel (Fig. 3b) is consistent with a DNA translocation model like that shown in Fig. 4a.

The recruitment of concatemeric DNA and the specific recognition of the *pac* site by nonameric gp3 might be initiated by DNA contact along the spikes of the gp3 nonamer at high ring radius. Such a model for *pac* site recognition would appear to be favored over monomer-initiated binding because of the very rapid self-assembly kinetics of gp3.²⁶ This hypothesis for nonamer/*pac* site recognition is particularly attractive given the apparent circumferential spacing between adjacent spikes of protein density (~34 Å), which is close to the contour length of one turn of the DNA helix (~33 Å pitch).³⁴ The model depicted in Fig. 4b would allow interaction of adjacent subunits of the ring with phosphate-binding sites along a single face of DNA. Bending of the 21-bp *pac* site by ~40° would be sufficient to facilitate cooperative binding of three neighboring

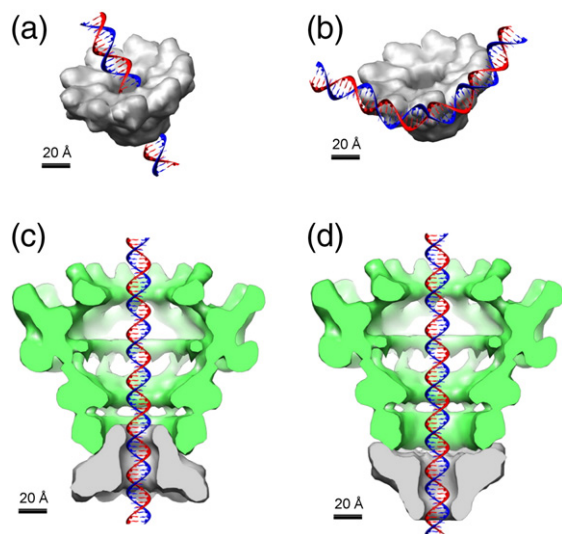


Fig. 4. Models for interaction of the gp3 ring assembly of Fig. 3 with double-stranded B DNA and the P22 portal. The dsDNA, terminase ring and portal vertex are plotted on the same scale. (a) Passage of dsDNA through the central hole of the gp3 ring assembly. (b) Binding of dsDNA to the periphery of the gp3 ring assembly. Docking of the funnel-shaped gp3 ring at the portal neck is depicted in neck-to-neck (c) and mouth-to-neck (d) orientations.

subunits of the gp3 nonamer, thus suggesting a plausible structural basis for *pac* site selection.

Studies of phages λ , T3, SPP1, and T4 provide strong evidence that the translocation of DNA into the procapsid is powered by the ATPase activity of the terminase large subunit. However, little is known about the molecular structures of the terminase motor components or the three-dimensional organization of its parts. To generate a force for DNA packaging, a terminase complex must be bound to the procapsid. In the phages λ and T4, current evidence indicates that the terminase large subunit binds directly to the portal protein of the procapsid during DNA packaging.^{35–37} These findings do not preclude additional contacts to the procapsid involving the terminase small subunit. In fact, for phages SPP1 and T3, experimental evidence has been obtained for direct procapsid contact by both the small and large subunits.^{2,5,38} A phylogenetic analysis of terminase large subunits of many phages suggests also that the terminase of P22 is most closely related to that of SPP1.³⁹ While it is not known if terminases of different phages bind to their respective procapsids via different or similar mechanisms, the possibility exists that both the large and small subunits of P22 terminase may make contact with the procapsid. Docking of the terminase ring at the portal vertex could thus provide an effective translocating channel, as noted above. Using the present and previous⁴⁰ EM reconstructions, we illustrate two feasible coaxial arrangements for such a DNA translocating channel in Fig. 4c and d. In both arrangements, the conical shape of the gp3 ring elongates the stalk of the portal that emerges from

the procapsid. While the models depicted in Fig. 4c and d allow for significant contact surfaces, it is not known whether a rigid or flexible interface would be required to accommodate the obvious symmetry mismatch between the two rings. It is conceivable, however, that a trio of subunits of the 9-fold gp3 ring could interact with a quartet of subunits of the 12-fold portal ring, since both have 120° radial spacing. In Fig. 4c and d, the end of the gp3 funnel that protrudes outwardly from the portal ring would presumably serve as the locus for contact with the terminase large subunit during ATPase- and DNase-directed activities. Because a lobe of portal subunit (gp1) density would extend beyond the gp3 ring in either Fig. 4c or d, both allow the terminase large subunit to simultaneously contact gp3 and gp1 subunits. Experiments in progress, which are designed to identify the gp3/gp2 and gp3/gp1 interaction surfaces, are expected to shed further light on the mode of portal docking.

Acknowledgements

Support of this research by National Institutes of Health (NIH) grants GM50776 (G.J.T.) and AI074825 (S.R.C.) is gratefully acknowledged. Electron microscopic imaging and reconstruction were conducted at the National Resource for Automated Molecular Microscopy, which is supported by the NIH through a P41 program grant (RR17573) from the National Center for Research Resources. We are grateful to Drs. Bridget Carragher and Clint Potter for their interest and helpful discussions during EM analysis. We also thank Prof. Peter E. Prevelige (University of Alabama at Birmingham) for providing resources for mass spectrometry of gp3 assemblies and contributing valuable discussions throughout the course of this work.

Supplementary Data

Supplementary data associated with this article can be found, in the online version, at [doi:10.1016/j.jmb.2008.08.050](https://doi.org/10.1016/j.jmb.2008.08.050)

References

1. Catalano, C. E. (2005). In *Viral Genome Packaging Machines: Genetics, Structure, and Mechanism* (Catalano, C. E., ed), Landes Bioscience/Eurekah.com and Kluwer Academic/Plenum Publishers. Georgetown, TX and New York.
2. Morita, M., Tasaka, M. & Fujisawa, H. (1995). Structural and functional domains of the large subunit of the bacteriophage T3 DNA packaging enzyme: importance of the C-terminal region in prohead binding. *J. Mol. Biol.* **245**, 635–644.
3. Gual, A., Camacho, A. G. & Alonso, J. C. (2000). Functional analysis of the terminase large subunit, G2P, of

- Bacillus subtilis* bacteriophage SPP1. *J. Biol. Chem.* **275**, 35311–35319.
4. Leffers, G. & Rao, V. B. (2000). Biochemical characterization of an ATPase activity associated with the large packaging subunit gp17 from bacteriophage T4. *J. Biol. Chem.* **275**, 37127–37136.
 5. Camacho, A. G., Gual, A., Lurz, R., Tavares, P. & Alonso, J. C. (2003). *Bacillus subtilis* bacteriophage SPP1 DNA packaging motor requires terminase and portal proteins. *J. Biol. Chem.* **278**, 23251–23259.
 6. Kondabagil, K. R., Zhang, Z. & Rao, V. B. (2006). The DNA translocating ATPase of bacteriophage T4 packaging motor. *J. Mol. Biol.* **363**, 786–799.
 7. Oliveira, L., Henriques, A. O. & Tavares, P. (2006). Modulation of the viral ATPase activity by the portal protein correlates with DNA packaging efficiency. *J. Biol. Chem.* **281**, 21914–21923.
 8. Draper, B. & Rao, V. B. (2007). An ATP hydrolysis sensor in the DNA packaging motor from bacteriophage T4 suggests an inchworm-type translocation mechanism. *J. Mol. Biol.* **369**, 79–94.
 9. Sun, S., Kondabagil, K., Gentz, P. M., Rossmann, M. G. & Rao, V. B. (2007). The structure of the ATPase that powers DNA packaging into bacteriophage T4 procapsids. *Mol. Cell.* **25**, 943–949.
 10. Casjens, S., Sampson, L., Randall, S., Eppler, K., Wu, H., Petri, J. B. & Schmiegler, H. (1992). Molecular genetic analysis of bacteriophage P22 gene 3 product, a protein involved in the initiation of headful DNA packaging. *J. Mol. Biol.* **227**, 1086–1099.
 11. Shinder, G. & Gold, M. (1988). The Nu1 subunit of bacteriophage λ terminase binds to specific sites in *cos* DNA. *J. Virol.* **62**, 387–392.
 12. Chai, S., Lurz, R. & Alonso, J. C. (1995). The small subunit of the terminase enzyme of *Bacillus subtilis* bacteriophage SPP1 forms a specialized nucleoprotein complex with the packaging initiation region. *J. Mol. Biol.* **252**, 386–398.
 13. Backhaus, H. (1985). DNA packaging initiation of *Salmonella* bacteriophage P22: determination of cut sites within the DNA sequence coding for gene 3. *J. Virol.* **55**, 458–465.
 14. Eppler, K., Wyckoff, E., Goates, J., Parr, R. & Casjens, S. (1991). Nucleotide sequence of the bacteriophage P22 genes required for DNA packaging. *Virology*, **183**, 519–538.
 15. Tye, B. K., Chan, R. K. & Botstein, D. (1974). Packaging of an oversize transducing genome by *Salmonella* phage P22. *J. Mol. Biol.* **85**, 485–500.
 16. Jackson, E. N., Jackson, D. A. & Deans, R. J. (1978). EcoRI analysis of bacteriophage P22 DNA packaging. *J. Mol. Biol.* **118**, 365–388.
 17. Wu, H., Sampson, L., Parr, R. & Casjens, S. (2002). The DNA site utilized by bacteriophage P22 for initiation of DNA packaging. *Mol. Microbiol.* **45**, 1631–1646.
 18. Streisinger, G., Emrich, J. & Stahl, M. M. (1967). Chromosome structure in phage T4, III Terminal redundancy and length determination. *Proc. Natl Acad. Sci. USA*, **57**, 292–295.
 19. Tavares, P., Lurz, R., Stiege, A., Ruckert, B. & Trautner, T. A. (1996). Sequential headful packaging and fate of the cleaved DNA ends in bacteriophage SPP1. *J. Mol. Biol.* **264**, 954–967.
 20. Lin, H., Simon, M. N. & Black, L. W. (1997). Purification and characterization of the small subunit of phage T4 terminase, gp16, required for DNA packaging. *J. Biol. Chem.* **272**, 3495–3501.
 21. Kondabagil, K. R. & Rao, V. B. (2006). A critical coiled coil motif in the small terminase, gp16, from bacteriophage T4: insights into DNA packaging initiation and assembly of packaging motor. *J. Mol. Biol.* **358**, 67–82.
 22. White, J. H. & Richardson, C. C. (1987). Gene 18 protein of bacteriophage T7. Overproduction, purification, and characterization. *J. Biol. Chem.* **262**, 8845–8850.
 23. Ortega, M. E. & Catalano, C. E. (2006). Bacteriophage lambda gpNu1 and *Escherichia coli* IHF proteins cooperatively bind and bend viral DNA: implications for the assembly of a genome-packaging motor. *Biochemistry*, **45**, 5180–5189.
 24. Maluf, N. K., Gaussier, H., Bogner, E., Feiss, M. & Catalano, C. E. (2006). Assembly of bacteriophage λ terminase into a viral DNA maturation and packaging machine. *Biochemistry*, **45**, 15259–15268.
 25. de Beer, T., Fang, J., Ortega, M., Yang, Q., Maes, L., Duffy, C. *et al.* (2002). Insights into specific DNA recognition during the assembly of a viral genome packaging machine. *Mol. Cell*, **9**, 981–991.
 26. Nemecek, D., Gilcrease, E. B., Kang, S., Prevelige, P. E., Jr, Casjens, S. & Thomas, G. J., Jr (2007). Subunit conformations and assembly states of a DNA-translocating motor: the terminase of bacteriophage P22. *J. Mol. Biol.* **374**, 817–836.
 27. Berjot, M., Marx, J. & Alix, A. J. P. (1987). Determination of the secondary structure of proteins from the Raman amide I band: the reference intensity profiles method. *J. Raman Spectrosc.* **18**, 289–300.
 28. Siamwiza, M. N., Lord, R. C., Chen, M. C., Takamatsu, T., Harada, I., Matsuura, H. & Shimanouchi, T. (1975). Interpretation of the doublet at 850 and 830 cm^{-1} in the Raman spectra of tyrosyl residues in proteins and certain model compounds. *Biochemistry*, **14**, 4870–4876.
 29. Arp, Z., Autrey, D., Laane, J., Overman, S. A. & Thomas, G. J., Jr (2001). Tyrosine Raman signatures of the filamentous virus Ff are diagnostic of non-hydrogen-bonded phenoxyls: demonstration by Raman and infrared spectroscopy of *p*-cresol vapor. *Biochemistry*, **40**, 2522–2529.
 30. Miura, T., Takeuchi, H. & Harada, I. (1989). Tryptophan Raman bands sensitive to hydrogen bonding and side-chain conformation. *J. Raman Spectrosc.* **20**, 667–671.
 31. Overman, S. A. & Thomas, G. J., Jr (1999). Raman markers of nonaromatic side chains in an alpha-helix assembly: Ala, Asp, Glu, Gly, Ile, Leu, Lys, Ser, and Val residues of phage fd subunits. *Biochemistry*, **38**, 4018–4027.
 32. Li, H. & Thomas, G. J. (1991). Cysteine conformation and sulfhydryl interactions in proteins and viruses. 1. Correlation of the Raman S–H band with hydrogen-bonding and intramolecular geometry in model compounds. *J. Am. Chem. Soc.* **113**, 456–462.
 33. Sousa, D. & Grigorieff, N. (2007). *Ab initio* resolution measurement for single particle structures. *J. Struct. Biol.* **157**, 201–210.
 34. Dickerson, R. E., Drew, H. R., Conner, B. N., Wing, R. M., Fratini, A. V. & Kopka, M. L. (1982). The anatomy of A-, B-, and Z-DNA. *Science*, **216**, 475–485.
 35. Frackman, S., Siegele, D. A. & Feiss, M. (1984). A functional domain of bacteriophage λ terminase for prohead binding. *J. Mol. Biol.* **180**, 283–300.
 36. Yeo, A. & Feiss, M. (1995). Specific interaction of terminase, the DNA packaging enzyme of bacteriophage lambda, with the portal protein of the prohead. *J. Mol. Biol.* **245**, 141–150.
 37. Lin, H., Rao, V. B. & Black, L. W. (1999). Analysis of capsid portal protein and terminase functional do-

- mains: interaction sites required for DNA packaging in bacteriophage T4. *J. Mol. Biol.* **289**, 249–260.
38. Fujisawa, H., Shibata, H. & Kato, H. (1991). Analysis of interactions among factors involved in the bacteriophage T3 DNA packaging reaction in a defined *in vitro* system. *Virology*, **185**, 788–794.
39. Casjens, S. R., Gilcrease, E. B., Winn-Stapley, D. A., Schicklmaier, P., Schmieger, H., Pedulla, M. L. *et al.* (2005). The generalized transducing *Salmonella* bacteriophage ES18: complete genome sequence and DNA packaging strategy. *J. Bacteriol.* **187**, 1091–1104.
40. Lander, G. C., Tang, L., Casjens, S. R., Gilcrease, E. B., Prevelige, P., Poliakov, A. *et al.* (2006). The structure of an infectious P22 virion shows the signal for headful DNA packaging. *Science*, **312**, 1791–1795.

Note added in proof. Recent refinements of the EM reconstructions of the nonameric rings formed by full-length gp3 and truncated gp3(Δ 1-127) have enabled marginally improved visualization of the difference electron density corresponding to the deleted C-terminal 35 residues. The results suggest that, in addition to localization along the channel surface (colored red in Fig. 3b), a portion of the C-terminal 128–162 sequence may extend above the mouth of the funnel proximal to the channel. This finding is consistent with the model proposed for nonspecific DNA recognition during translocation (Figs. 4c and d). Further details of the molecular mechanism will depend upon obtaining EM reconstructions of significantly improved resolution. Such studies are currently in progress.